The Effects of Interfacial Properties on the Mechanical Behavior of Layered Aluminum Matrix Composites

H. Ismar, F. Schröter, F. Streicher

Al/SiC-composites are not only affected by inelastic deformation processes in the metallic matrix but also by debonding occurring at the fiber-matrix-interface. Therefore a viscoplastic material law including damage evolution and growth, as well as a cohesive zone model for the interface, are integrated into a finite element technique. By this the influence of interfacial characteristics on the stress-strain behavior of a laminated Al/SiC-composite is examined.

1 Introduction

Composite properties are commonly extremely affected by the behavior of the interface between the reinforcements and the matrix. Thus ceramic matrix composites (CMC) are mostly designed with a sufficiently weak interface allowing debonding processes and therefore energy absorption by frictional sliding during loading (Ismar and Streicher, 1999). Thus the composite deforms in a "pseudo-plastic" manner connected with a considerable ductility.

On the contrary, the deformation behavior of metal matrix composites (MMC) is dominated by inelastic deformation processes in the matrix involved in energy absorption via dislocation motion. Therefore the opportunity of enhancing ductility by energy-absorbing processes at the interface is only used when improving the toughness of relatively brittle metals such as zinc (Vescera et al., 1991). Nevertheless the interface between metallic matrix and reinforcements is usually preferred to be strong so that the inelastic deformation of the matrix is not hindered.

For these reasons modeling of fiber reinforced MMCs has to take into account inelastic matrix deformation as well as debonding processes at the interface. Especially when examining complex loadings, such as cyclic or multiaxial loads, special attention has to be focused on the realistic reproduction of the thermomechanical behavior of metals observable during experimental tests. Therefore a viscoplastic material law based on Chaboche's (1977) constitutive model is employed and extended in order to consider inelastic volume changes during cyclic loading as well as ductile damage at high inelastic straining. This material model is presented in section 2.

A multitude of models exists to predict the mechanical behavior of metals. Thus studies of the past decade recommend a couple of models to capture the nonlinear interfacial behavior in MMCs. Very popular interfacial models are based on the assumptions of an interface completely debonded from the initial or a weak interface supposing an unhindered ability of transferring normal compressive stresses and an either entire or partial non-transfer of normal tensile stresses in the interface. These models were applied by Sherwood and Quimby (1995) and Bonora et al. (1994) who investigated the behavior of reinforced titanium-alloys. These simple models are easily incorporated into a finite element analysis by using contact surfaces or gap and spring elements and offer the possibility of being enhanced by including also frictional sliding (Dragone, 1991). Zahl (1993) describes the interface in Al/Al_2O_3-composites with a thin layer of perfectly plastic material with constant thickness thus representing a shearable interface able to transmit any stress level normal to the fiber without yielding or debonding.

A more concise approach to capture the interfacial response is made feasible by the cohesive zone models founded by Needleman (1987) and supplemented by several researchers (Tvergaard, 1990; Lissenden and Herakovich, 1995; Chaboche et al., 1997; Siegmund and Brocks, 1998). As far as MMCs are concerned, the cohesive zone model was used to investigate the effect of fiber debonding in discontinuously reinforced aluminum alloys (Tvergaard, 1990), the influence of residual stresses on Al-SiC composites (Povirk et al., 1991), and the dynamic crack growth running along the interface in a bi-material with lamellar arrangement of phases (Siegmund et al., 1997).

But as far as MMCs are concerned it has to be borne in mind that the interface properties such as strength and toughness are extremely affected by the manufacturing process so that experimental investigations establish very different interfacial characteristics. The current study investigates the general influence of interfacial characteristics on the overall mechanical behavior rather than absolutely accurately predicting the resulting composite properties.

By combining the material laws for the single phases with a numerical procedure, such as the finite element method, we achieve an efficient tool for predicting how certain fundamental variables, such as properties of phases, the fiber arrangement of phases, or the manufacturing process, affect the mechanical behavior of MMCs. In the underlying study this is especially shown for an aluminum alloy reinforced bidirectionally with SiC-fibers.

2 Viscoplastic Material Model for the Matrix

The constitutive equations of metallic materials should take into account the most important effects of inelastic deformation such as the increase of the yield stress with increasing deformation, rate- and time-dependency, the Bauschinger-effect (the premature inelastic deformation after a change of the loading direction) and the hysteresis loops under cyclic loading conditions. Therefore, an extended version of the unified viscoplastic material model of Chaboche (1977) was used to describe the metallic matrix in the composite. By expanding this model with the transition flow potential (TFP) a constitutive theory is obtained which is also able to describe changing yield surface geometry and accompanying inelastic volume changes as they were observed by Ismar and Schmitt (1990) at the beginning of the inelastic deformation after a purely elastic loading period.

Additionally ductile damage caused by a strong inelastic deformation influences the mechanical behavior of the metallic matrix and, therefore, has to be considered too. Damage is here introduced by Kachanov's (1958) concept of effective stress

$$\tilde{\sigma}_{ij} = \frac{\sigma_{ij}}{1 - \omega} \tag{1}$$

where σ_{ij} are the components of the stress tensor and ω is a scalar variable of damage caused by the formation of microdefects, such as microcracks and microvoids. This scalar definition of damage implies the similarity of the mechanical response under compression and tension. But, as Hansen and Schreyer (1995) stated, the microdefects may partially close in compression leading to a deactivated damage status. Therefore, an active damage variable

$$\tilde{\omega} = \omega \left[\Theta(I_1^\sigma) + H \left(1 - \Theta(I_1^\sigma) \right) \right] = \left\{ \begin{array}{ll} \omega & : I_1^\sigma \geq 0 \\ H\omega & : I_1^\sigma < 0 \end{array} \right. \tag{2}$$

is considered here. $\Theta(\cdot)$ represents the Heaviside function, $I_1^\sigma = \sigma_{ii}$ the first invariant of the stress tensor, and H the so-called microcrack closure parameter with $0 \leq H \leq 1$.

Presuming small deformations the total strain rate tensor $\dot{\varepsilon}_{ij}$ is a linear superposition of an elastic $\dot{\varepsilon}_{ij}^e$, a thermal $\dot{\varepsilon}_{ij}^t$, and an inelastic component $\dot{\varepsilon}_{ij}^i$, i.e.

$$\dot{\varepsilon}_{ij} = \dot{\varepsilon}_{ij}^e + \dot{\varepsilon}_{ij}^t + \dot{\varepsilon}_{ij}^i \tag{3}$$

Considering the principle of strain equivalence (e.g. Lemaitre, 1992), stating that any strain constitutive equation for the damaged material is derived by substituting the stress by the effective stress in the equations of the virgin material, the law of linear thermoelasticity of the damaged material is obtained:

$$\dot{\varepsilon}_{ij}^e + \dot{\varepsilon}_{ij}^t = \frac{1}{E(1 - \omega)} \left((1 + v)\dot{\sigma}_{ij} - v\dot{\sigma}_{kk}\delta_{ij} \right) + \alpha^t \dot{T}\delta_{ij} \tag{4}$$

with the temperature T and the temperature-dependent material parameters Young's modulus $E = E(T)$, Poisson's ratio $v = v(T)$, and the coefficient of thermal expansion $\alpha^t = \alpha^t(T)$.

In order to couple damage constitutive equations also with the viscoplastic equations, an inelastic potential is defined in the effective stress space:

$$\Omega = \frac{K}{N+1} \left\langle \frac{\tilde{s}_v(\tilde{s}_{ij}) - r}{K} \right\rangle^{N+1} = \frac{K}{N+1} \left\langle \frac{\tilde{s}_o}{K} \right\rangle^{N+1} \tag{5}$$

where K and N are material parameters, $\langle . \rangle$ the Macauley bracket, and $\tilde{s}_{ij}$ the components of the effective active stress tensor

$$\tilde{s}_{ij} = \tilde{\sigma}_{ij} - \sum_{k=1}^{m} x_{ij}^k \tag{6}$$

which can be interpreted as the difference between the components of the effective stress tensor and several kinematic hardening variables x_{ij}^k. The effective active equivalent stress $\tilde{s}_v$ will be discussed below. By the condition

$$\tilde{s}_v(\tilde{s}_{ij}) - r = \tilde{s}_o \leq 0 \tag{7}$$

the elastic domain (potential surface with $\Omega = 0$) is defined. In eq. (7) r is the isotropic hardening and $\tilde{s}_o$ the effective overstress, which is a measure for the distance between the effective stress point and the corresponding point of the elastic domain.

Applying the kinetic equation we receive the components of the inelastic strain rate

$$\dot{\varepsilon}_{ij}^i = \frac{\partial \Omega}{\partial \tilde{s}_{ij}} = \underbrace{\left\langle \frac{\tilde{s}_o}{K} \right\rangle^N}_{\dot{\varepsilon}_v^i} \frac{\partial \tilde{s}_v}{\partial \tilde{s}_{ij}} \frac{\partial \Omega}{\partial \tilde{s}_{ij}} \tag{8}$$

where $\dot{\varepsilon}_v^i$ marks the equivalent inelastic strain rate.

Commonly the inelastic deformation of metals is described by using the v. Mises potential, which is based on the hypothesis of inelastic incompressibility. As mentioned before, recent investigations on certain materials have shown that inelastic volume changes occur at the beginning of the inelastic deformation. Therefore, the viscoplastic model was improved by implementing the transition flow potential (TFP) formulated by Mahrenholtz and Ismar (1979). Thus, we receive for the equivalent effective active stress

$$\tilde{s}_v = \sqrt{\frac{\left(\chi I_1^{\tilde{s}}\right)^2 + 6 I_2^{\tilde{s}'}}{\chi^2 + 2}} \tag{9}$$

with the first invariant of effective active stress $I_1^{\tilde{s}} = \tilde{s}_{ii}$ and the second invariant of effective active stress deviator $I_2^{\tilde{s}'} = \frac{1}{2} \tilde{s}_{ij}' \tilde{s}_{ij}'$.

The internal variable χ can be interpreted as the ratio of the small (r_1) to the large (r_2) half axis of an ellipsoid of revolution-shaped potential surface and is dependent on the inelastic strain of the respective load cycle, see Fries et al. (1997), causing a degeneration of the yield surface to the well-known v. Mises surface with growing inelastic strain of the respective cycle.

Moreover, the variables of kinematic and isotropic hardening have to be defined. A good representation of the cyclic hardening behavior of metallic materials can be obtained by modifying the usual linear kinematic hardening rule (Prager's rule) with a saturation term. Furthermore, thermal recovery effects

appearing at elevated temperature can be incorporated. Thus we receive

$$\dot{x}_{ij}^k = \frac{(\chi^2 + 2)}{3} C^k \left(1 - \tilde{\omega}\right) \dot{\varepsilon}_{ij}^i - \Gamma^k \left(1 - \tilde{\omega}\right) \dot{\varepsilon}_v^i x_{ij}^k - \underbrace{\Gamma^{rk} \left(x_v^k\right)^{M^k - 1} x_{ij}^k}_{\text{thermal recovery}} \tag{10}$$

Herein C^k, Γ^k, Γ^{rk}, and M^k are material constants and x_v^k is an equivalent value of the kinematic hardening tensor. As the index k indicates, serval kinematic hardening terms of the same type are superposed allowing a greater flexibility in the adaption of the kinematic hardening on the material behavior.

The hardening model is complemented by the isotropic hardening r causing an expansion of the yield surface. This evolves according to

$$\dot{r} = B \left(Q - r\right) \left(1 - \tilde{\omega}\right) \dot{\varepsilon}_v^i - \underbrace{\Gamma^r \left(r - Q^r\right)}_{\text{thermal recovery}} \tag{11}$$

starting from the value $r(\varepsilon_v^i = 0) = R_0$. B, Q, Q^r, and Γ^r are material parameters.

Finally, the growth of damage is given by (Lemaitre, 1992)

$$\dot{\omega} = \frac{g}{S} \dot{\varepsilon}_v^i \Theta(\varepsilon_v^i - \varepsilon_{v0}^i) \tag{12}$$

where ε_{v0}^i is the equivalent inelastic strain below which no damage occurs, S a material parameter, and g the damage energy release rate

$$g = \frac{1}{2E(1 - \tilde{\omega})} \left((1 + \nu) I_2^{\sigma'} + \frac{1 - 2\nu}{3} \left(I_1^\sigma\right)^2 \right) \tag{13}$$

Therewith the material law is completed.

3 Interface Constitutive Model

The cohesive zone approach of Needleman (1987) with enhancements of Tvergaard (1990) and Lissenden and Herakovich (1995) models the separation of two phases along a predefined process zone by defining an interface potential specifying the dependence of the tractions in the interface consisting of normal and tangential components T_n, T_{t1}, and T_{t2} upon the corresponding discontinuity in the displacement field across the interface:

$$\overrightarrow{\Delta u} = \begin{bmatrix} \Delta u_n \\ \Delta u_{t1} \\ \Delta u_{t2} \end{bmatrix} = \overrightarrow{u_\beta} - \overrightarrow{u_\alpha} \tag{14}$$

where $\overrightarrow{u_\beta}$ and $\overrightarrow{u_\alpha}$ are the displacement vectors at the interior and the exterior borders of the interface zone as displayed in Figure 1. Needleman assumed a potential reflecting the non-linear variations in T_n represented by a function, which evolves from the value 0 at $u_n = 0$ through a maximum value σ_{max} again down to the value 0 at $u_n = \delta_n$, which is assigned to final separation.
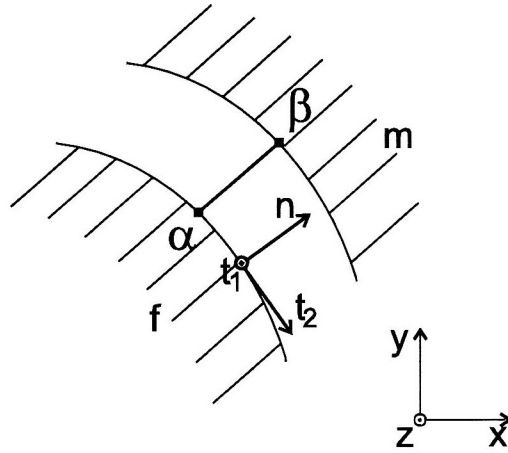
Figure 1. Interface Coordinate System

In order to capture the coupling between normal and tangential debonding a dimensionless parameter

$$\lambda = \sqrt{\left(\frac{\langle u_n \rangle}{\delta_n}\right)^2 + \left(\frac{u_{t1}}{\delta_t}\right)^2 + \left(\frac{u_{t2}}{\delta_t}\right)^2} \tag{15}$$

is introduced, where the Macauley bracket $\langle \cdot \rangle$ specifies that under compressive loading ($u_n \leq 0$) debonding occurs only in tangential direction. The characteristic lengths δ_n and δ_t are material parameters which correspond to the work of separation in connection with the maximum interface strength σ_{max}. $\lambda = 0$ marks the completely intact interface whereas for values $\lambda \geq 1$ no more cohesive stresses can be supported.

The nonlinear relations between traction and displacement difference depend upon the maximum value of λ in the course of the precedent loading history, λ_{max}, in order to prevent healing of the interface with decreasing values of λ.

For $\lambda_{max} < 1$ the relations

$$
\begin{aligned}
T_n &= \begin{cases} \frac{27}{4}\sigma_{\max} \frac{u_n}{\delta_n} & \text{for } u_n \leq 0 \\ F(\lambda_{max})\frac{u_n}{\delta_n} & \text{for } u_n > 0 \end{cases} \\
T_{t1} &= \alpha F(\lambda_{max})\frac{u_{t1}}{\delta_t} \\
T_{t2} &= \alpha F(\lambda_{max})\frac{u_{t2}}{\delta_t}
\end{aligned}
\tag{16}
$$

can be established with a monotonically decreasing function

$$F(\lambda) = \frac{27}{4}\sigma_{max}(1 - \lambda)^2 \tag{17}$$

Thus we have a maximum normal traction of σ_{max}, whereas the maximum tangential traction is $\alpha\sigma_{max}$. Under compressive normal loading ($u_n < 0$) a sufficiently high stiffness of $\frac{27}{4}\sigma_{max}$ prevents penetrating of the fiber and the matrix phases.

After complete debonding characterized by $\lambda_{max} \geq 1$ the interface is still capable of transmitting compressive and tangential tractions due to contact and friction. Thus for $\lambda_{max} \geq 1$ we use

$$T_n = \begin{cases} \frac{27}{4}\sigma_{max}\frac{u_n}{\delta_n} & \text{for } u_n \leq 0 \\ 0 & \text{for } u_n > 0 \end{cases}$$

$$T_{t1} = \begin{cases} -sgn(\dot{u}_{t1})\mu T_n & \text{for } u_n \leq 0 \\ 0 & \text{for } u_n > 0 \end{cases} \tag{18}$$

$$T_{t2} = \begin{cases} -sgn(\dot{u}_{t2})\mu T_n & \text{for } u_n \leq 0 \\ 0 & \text{for } u_n > 0 \end{cases}$$

to describe tangential sliding, where μ is the friction coefficient.

But for $\sqrt{T_{t1}^2 + T_{t2}^2} < \mu|T_n|$, i.e. the resultant of the tangential tractions is less than Coulomb's friction limit, no sliding occurs and the interface behavior is simulated by elastic springs:

$$T_{t1} = \begin{cases} \frac{4\mu|T_n|}{\delta_t}\dot{u}_{t1} & \text{for } u_n \leq 0 \\ 0 & \text{for } u_n > 0 \end{cases} \tag{19}$$

$$T_{t2} = \begin{cases} \frac{4\mu|T_n|}{\delta_t}\dot{u}_{t2} & \text{for } u_n \leq 0 \\ 0 & \text{for } u_n > 0 \end{cases}$$

with the stiffness $4\mu|T_n|/\delta_t$. A change from eq. (18) to eq. (19) occurs when the resultant of $\dot{u}_{t1}$ and $\dot{u}_{t2}$ changes sign.

Figure 2 schematically displays the behavior defined by this cohesive model by means of two examples under different loading conditions. Finally it should be pointed out that Chaboche et al. (1997) criticize the physically non-acceptable non-monotonous stiffness evolution at the beginning of sliding. But nevertheless the cohesive zone model accomplishes a useful aid when examining the influence of interfacial properties in MMCs.
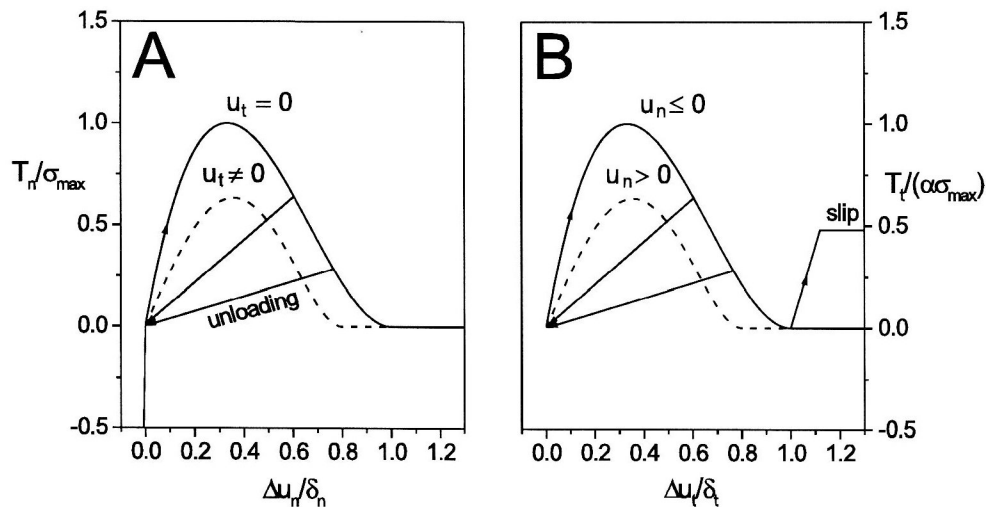
Figure 2. Interface Constitutive Equations under Purely Normal Tensile (A) and Tangential (B) Loading

4 Finite Element Formulation

In order to study a MMC laminate a three-dimensional geometric model is necessary. Thus strain coupling effects between the single plies can be taken into account. Here a laminate of the antisymmetric fiber layup $[0°/90°]$ is considered. By assuming appropriate geometric idealizations, such as the equidistant arrangement of circular cylindrical fibers, a unit cell is derived which contains two quarters of fibers. The monofilament fiber has a diameter of $D_f = 140\,\mu m$. The fiber volume fraction is fixed at 32%.

The finite element mesh shown in Figure 3 consists of 780 brick continuum elements and 132 bar-formed interface elements connecting corresponding nodes of the fiber and the matrix phases. Boundary conditions require that all external surfaces of the unit cell remain plane and parallel to the original configuration. The viscoplastic material model was implemented into the finite element package MARC in form of a user-supplied material model, whereas a special interface element was developed in order to capture the interfacial debonding (Schröter, 1999).

The metallic matrix of the composite is formed by an AlMgSi1-aluminum alloy, the elastic and viscoplastic material parameters of which were experimentally determined at our laboratories (Ismar and Penth, 1998). Damage parameters were taken form Lemaitre (1992). As the SiC-fibers, which deform purely elastically, show very different elastic and thermal properties thermal residual stresses arising during manufacture have also to be considered in the simulation.

Among the parameters defining the interfacial model, only the characteristic lengths are fixed at a fractional amount of the fiber diameter: $\delta_n = \delta_t = 0.01 \cdot D_f$. All other parameters are varied in order to analyze their effects on the composite mechanical behavior.
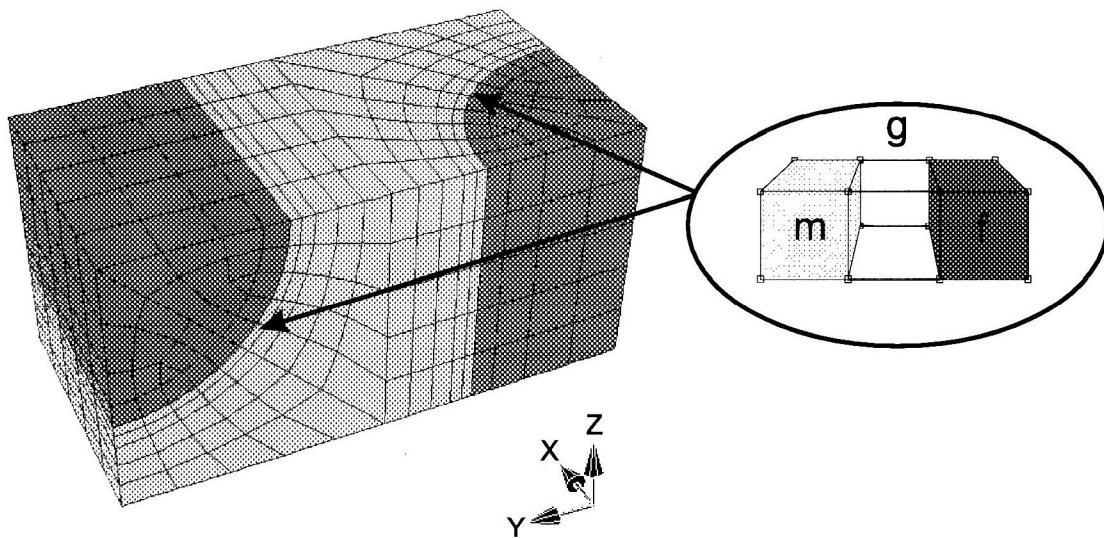
Figure 3. Finite Element Unit Cell

5 Numerical Results

Primarily we consider the laminate loaded by a displacement-controlled monotonous tensile load parallel to the fiber oriented in z-direction ($[0°]$-fiber) in Figure 3. Next the interfacial properties are fixed at $\sigma_{max} = 200$ MPa and $\alpha = 1$, where α specifies the relation between the tangential and the normal interfacial strength.

The process of interfacial debonding is illustrated in the left part of Figure 4. Using a 20-times magnification of displacements it can be seen that the debonding is concentrated at the pole of the transversely loaded x-fiber ($[90°]$-fiber). Investigating a certain point of the interface, the extent of debonding grows with increasing external load as well as the separation between fiber and matrix in circumferential direction. The right part of Figure 4 summarizes the normalized displacement difference $\Delta u_n/\delta_n$ determined

at the pole of the [90°]-fiber, which obviously grows over-proportionally with increasing external strain caused by the decreasing "stiffness" of the interface.

A

ε = 0.0 %

ε = 0.1 %

ε = 0.3 %

ε = 0.5 %

(displacements 20-times magnificated)

B
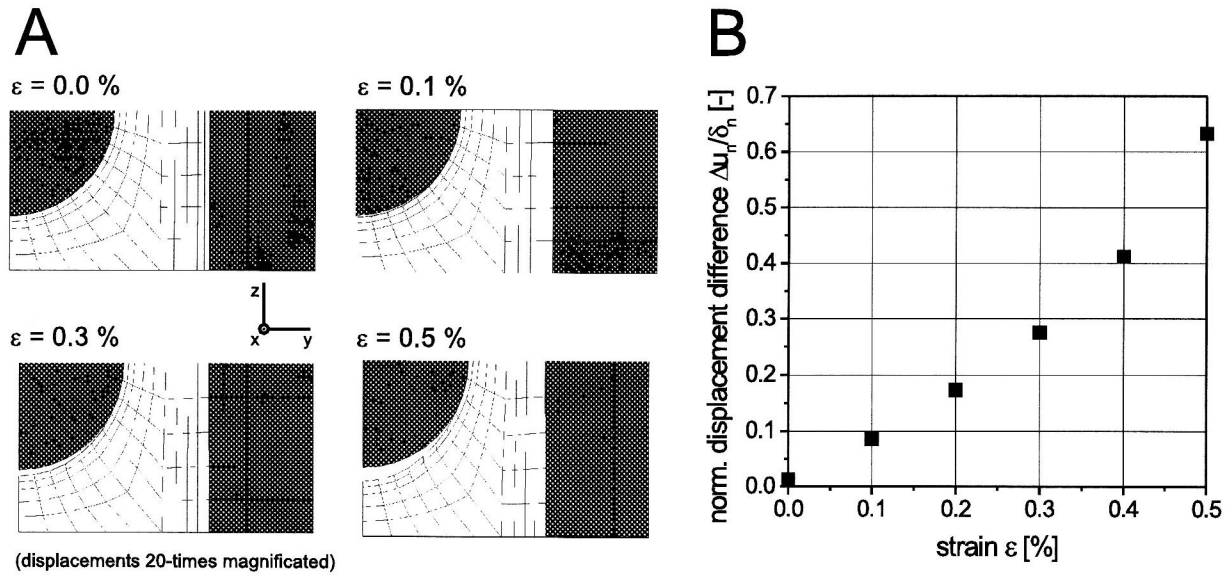
Figure 4. Debonding during Monotonic Tensile Loading (A) and Normalized Normal Displacement Difference $\frac{\Delta u_n}{\delta_n}$ at the Pole of the 90°-Fiber (B),$\sigma_{max} = 200\,\mathrm{MPa}$, $\alpha = 1$

Evidently the process of interfacial debonding influences the macroscopic stress-strain curves of the laminate. In the left field Figure 5 compares the mechanical behavior for various interfacial normal strengths σ_{max} whereby α is kept constant. Furthermore the behavior of the laminate with a perfectly bonded interface computed by assigning σ_{max} to a very high value is incorporated. It can be noticed that the curve associated with $\sigma_{max} = 400$ MPa closely coincides with the curve of the perfect interface. This is due to the inelastic matrix flow hindering the formation of higher stresses in the interface. Thus the interface in an Al/SiC-composite can be estimated to behave like a perfect interface if its strength exceeds 400 MPa. Furthermore it should be mentioned that the tension-compression-asymmetry of the interfacial model induces also a tension-compression-asymmetry in the stress-strain-diagrams of the composite (Schröter, 1999).
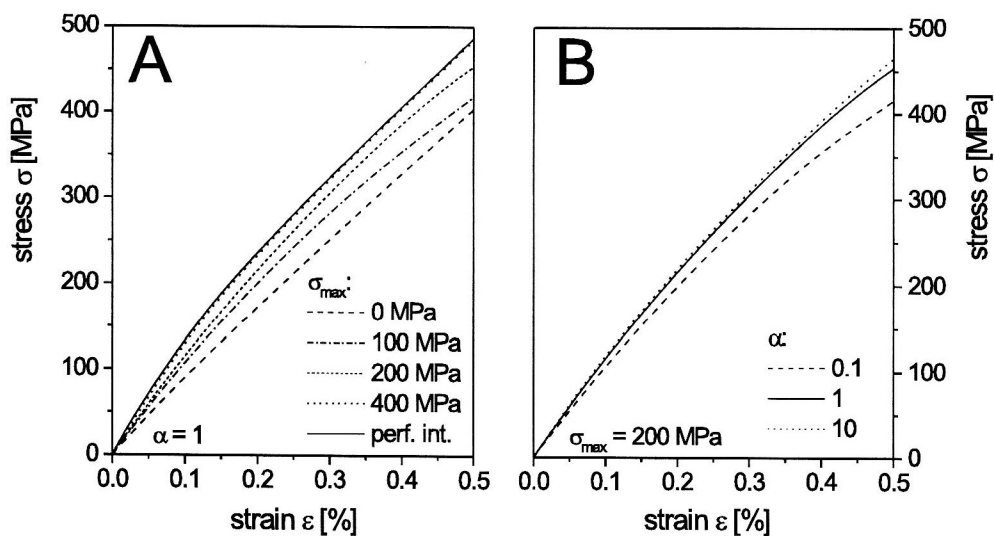
Figure 5. Tensile Stress-Strain Behavior of the Laminate depending on σ_{max} at $\alpha = 1$ (A) and on α at $\sigma_{max} = 200$ MPA (B)

The right field of Figure 5 displays the effect of varying α, the ratio of the tangential to the normal interfacial strength, on the stress-strain behavior assuming a constant σ_{max} of 200 MPa. Starting from identical interfacial strengths in normal and tangential directions ($\alpha = 1$) a drastic increase of the tangential strength to $\alpha = 10$ does not significantly raise the stiffness and strength of the laminate. On the contrary, decreasing the tangential strength to $\alpha = 0.1$ a conspicuous reduction of the composite strength and stiffness can be noticed.

Secondly the unit cell is exposed to a cyclic mechanical load of the macroscopic strain amplitude $\Delta\varepsilon = 0.2\%$ at an elevated temperature of 100°C. Thereby 40 cycles are examined. Figure 6 shows the inelastic performance density dissipated by the composite per cycle for the two cases of a perfect interface and a limited interfacial strength of $\sigma_{max} = 200$ MPa and $\alpha = 1$. It is obvious that a decreasing interfacial strength reduces the extent of inelastic deformation in the matrix due to limited stress transfer across the interface. Moreover, considering the lower interfacial strength, the inelastic performance density declines more quickly in the course of the cycles. Therefore it can be assumed that a composite with limited interfacial strength reduces the probability of matrix fatigue failure. But on the other hand strength and stiffness of the laminate are evidently affected in a negative way.
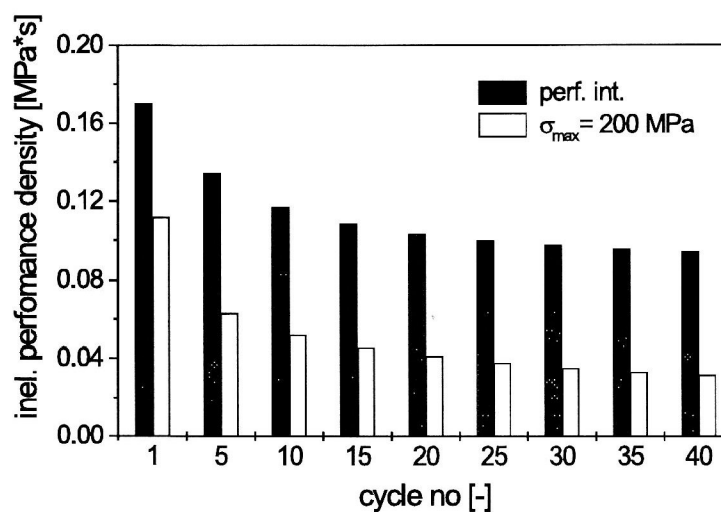
Figure 6. Inelastic Performance Density per Cycle in the Course of Loading for a Perfect Interface and One with $\sigma_{max} = 200$ MPa and $\alpha = 1$

6 Concluding Remark

The current paper examines the mechanical behavior of cross-ply reinforced aluminum matrix composites under usage of a model, which takes into account viscoplastic matrix deformation as well as interfacial debonding. The study focuses on the influence of interfacial properties on the macroscopic response of the laminate. Thus it hopefully offers valuable hints to material scientists how to choose interfacial properties for achieving particular composite properties.

Literature

1. Bonora, N.; Costanzi, M.; Newaz, G.; Marchetti, M.: Microdamage effect on the overall response of long fibre/metal-matrix composites. Composites, 25, (1994), 575–582.

2. Chaboche, J.L.: Viscoplastic constitutive equations for the description of cyclic and anisotropic behaviour of metals. Bull. Acad. Pol. Sci. Ser. Sci. Tech., 25, (1977), 33–42.

3. Chaboche, J.L.; Girard, R.; Levasseur, P.: On the interface debonding models. J. Damage Mech., 6, (1997), 220–257.

4. Dragone, T.L.: Effects of interface properties on the mechanical behavior of short fiber reinforced metal matrix composites. 32nd Structures, Structural Dynamics and Materials Conference, Baltimore, AIAA-91-0981-CP, (1991), 87–94.

5. Fries, V.; Ismar, H.; Penth, M.: Inelastic deformation behaviour of AlMgSi1. Mech. Res. Co., 24, (1997), 359–370.

6. Hansen, N.R.; Schreyer, H.L.: Damage Deactivation. J. Appl. Mech., 62, (1995), 450–458.

7. Ismar, H.; Schmitt, J.: Zur zyklischen Belastung einer Aluminiumlegierung im Bereich kleiner plastischer Formänderungen. ZAMM, 70, (1990), T324–T327.

8. Ismar, H.; Penth, M.: Comportement inélastique de l'alliage AlMgSi1 avec prise en compte des effects liés au chargement et à la restauration dépendant du temps. Eur. Phys. J. AP, 2, (1998), 27–34.

9. Ismar, H.; Streicher, F.: Modelling and simulation of the mechanical behavior of ceramic matrix composites as shown by the example of SiC/SiC. Comput. Mat. Sci., 16, (1999), 17–24.

10. Kachanov, L.M.: Time of the rupture process under creep conditions. Izv Akad Nauk S.S.R. Otd. Tekh Nauk, 8, (1958), 26–31.

11. Lemaitre, J.: A course on damage mechanics. Springer, Berlin et al., (1992).

12. Lissenden, C.F.; Herakovich, C.T.: Numerical modelling of damage development and viscoplasticity in metal matrix composites. Comput. Methods Appl. Mech. Engrg., 126, (1995), 289–303.

13. Mahrenholtz, O.; Ismar, H.: Ein Modell des elastisch-plastischen Übergangsverhaltens metallischer Werkstoffe. Abh. Braunsch. Wiss. Ges., 30, (1979), 138–144.

14. Needleman, A.: A continuum model for void nucleation by inclusion debonding. J. Appl. Mech., 54, (1987), 525–531.

15. Povirk, G.L.; Needleman, A.; Nutt, S.R.: An analysis of the effect of residual stresses on deformation and damage mechanisms in Al-SiC composites. Mat. Sci. & Eng., A132, (1991), 31–38.

16. Schröter, F.: Numerische Simulationen zu bidirektional mit Langfasern verstärktem Aluminium unter Nutzung gekoppelter Ansätze zur Erfassung von Viskoplastizität und Schädigung. Bad Iburg, (1999).

17. Sherwood, J.A.; Quimby, H.M.: Micromechanical modeling of damage growth in titanium based metal-matrix composites. Comput. & Struct., 56, (1995), 505–514.

18. Siegmund, T.; Fleck, N.A.; Needleman, A.: Dynamic crack growth across an interface. Int. J. Fract., 85, (1997), 381–402.

19. Siegmund, T.; Brocks, W.: Tensile deformation by local failure criteria. Tech. Mech., 18, (1998), 261–270.

20. Tvergaard, V.: Effect of fibre debonding in a whisker-reinforced metal. Mat. Sci. & Eng., A125, (1990), 203–213.

21. Vescera, F.; Keustermans, J.P.; Dellis, M,A.; Lips, B.; Delannay, F.: Processing and properties of Zn-Al alloy matrix composites reinforced by unoriented fibres. In: Metal matrix composites – Processing, microstructure and properties, 12th Risø Int. Symp. on Materials Sci., eds: Hansen, N.; Jensen, D.J.; Leffers, H.; Lilholt, T.; Lorentzen, A.S.; Pedersen, A.S.; Pedersen, O.B.; Ralph, B., Roskilde, Denmark, (1991), 719–724.

22. Zahl, D.B.: The effect of interfacial sliding on the strength of metal matrix composites. Comput. Mat. Sci., 1, (1993), 249–258.

Address: Prof. Dr.-Ing. H. Ismar, Dr.-Ing. F. Schröter, Dipl.-Ing. F. Streicher, Lehrstuhl für Technische Mechanik, Naturwissenschaftlich-Technischer Fachbereich III, Universität des Saarlandes, Postfach 15 11 50, D-66041 Saarbrücken